ACS Catalysis

Research Article

pubs.acs.org/acscatalysis

Tetrahexahedral Pt Nanocrystal Catalysts Decorated with Ru Adatoms and Their Enhanced Activity in Methanol Electrooxidation

Hai-Xia Liu,[†] Na Tian,*[,†] Michael P. Brandon,[‡] Zhi-You Zhou,[†] Jian-Long Lin,[†] Christopher Hardacre,[‡] Wen-Feng Lin,*[,‡] and Shi-Gang Sun*[,†]

[†]State Key Laboratory of Physical Chemistry of Solid Surfaces, Department of Chemistry, College of Chemistry and Chemical Engineering, Xiamen University, Xiamen, 361005, China

[‡]Centre for the Theory and Application of Catalysis (CenTACat), School of Chemistry and Chemical Engineering, Queen's University Belfast, Belfast BT9 5AG, U.K.

Supporting Information

ABSTRACT: Tetrahexahedral Pt nanocrystals (THH Pt NCs) bound by well-defined high index crystal planes offer exceptional electrocatalytic activity, owing to a high density of low-coordination surface Pt sites. We report, herein, on methanol electrooxidation at THH Pt NC electrodes studied by a combination of electrochemical techniques and in situ FTIR spectroscopy. Pure THH Pt NC surfaces readily facilitate the dissociative chemisorption of methanol leading to poisoning by strongly adsorbed CO. Decoration of the stepped surfaces by Ru adatoms increases the tolerance to poisoning and thereby reduces the onset potential for methanol oxidation by over 100 mV. The Ru modified THH Pt NCs exhibit greatly superior catalytic currents and CO_2 yields in the low potential range, when compared with a commercial PtRu alloy nanoparticle catalyst. These results are of fundamental importance in terms of model nanoparticle electrocatalytic systems of stepped surfaces and also have practical significance in the development of surface tailored, direct methanol fuel cell catalysts.

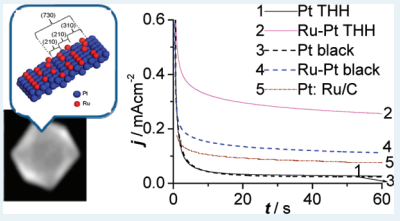

KEYWORDS: *tetrahexahedral platinum, high index facets, Ru adatoms, electrocatalysis, methanol electrooxidation, fuel cells*

1. INTRODUCTION

In recent years much research effort has been devoted to direct alcohol fuel cells (DEFCs) as part of the drive to develop environmentally benign and sustainable systems of energy generation.[1−5] The most progress has been made with the direct methanol fuel cell (DMFC) to the extent that there are now some commercially available units of this type with power outputs of up to 250 W.[6,7] Unfortunately, the methanol oxidation reaction (MOR) at the anode and the oxygen reduction reaction (ORR) at the cathode both suffer from slow kinetics, and currently high loadings of expensive Pt based catalysts are required to achieve acceptable current densities at low operating temperatures (<100 °C). The associated cost renders prohibitive the widespread commercial uptake of DMFCs.[6,8] Therefore, there is a need for continuing fundamental studies of Pt catalysts, with the goal of optimizing electrocatalytic performance, while minimizing the required quantities of precious metal.

To this end, Sun and co-workers have devised an electrochemical method for the preparation of high quality Pt (and Pd) nanocrystals bounded by facets of high Miller indices.[9,10] Of particular interest have been tetrahexahedral Pt nanocrystals (THH Pt NCs);[11] this shape may be visualized as a cube with a square based pyramid atop each of the six faces. TEM analysis indicated that these crystals were bounded mainly by {730} facets, with some {210}, {310}, or {520} planes also present. For a Pt {730} crystal plane, 43% of the surface atoms reside in step positions. This high density of low-coordination step atoms is particularly relevant to catalytic applications, since single crystal electrode studies have shown that atomic steps, kinks, and ledges are active sites for bond cleavage.[12] The expectation of high catalytic activity was borne out by experiment, with about 81 nm diameter THH Pt NCs exhibiting significantly lower onset potentials, and current densities up to 4 times greater than those generated by a commercial Pt/C (3.2 nm diam.) catalyst for formic acid and ethanol electrooxidation.[11] This ability to routinely and simply produce high index faceted Pt NCs offers the exciting possibility of transferring some of the wealth of knowledge gained in single crystal electrode studies to the solution of problems in the area of practical electrocatalysis.[13,14]

Efficient operation of a DMFC requires complete oxidation of the fuel to CO_2 at low anode potentials. Pt is indisputably the best monometallic catalyst for the MOR, facilitating the adsorption and dehydrogenation of methanol.[15,16] Despite being the most elementary alcohol, the exact electrooxidation mechanism for methanol is complex, involving a range of adsorbed intermediates, side reactions, products, and by-products. A early established concept[17] is that of parallel

Special Issue: Electrocatalysis

Received: December 25, 2011
Revised: March 3, 2012
Published: March 16, 2012

pathways to CO_2; a direct route through formaldehyde and formic acid, and an indirect pathway involving dissociative chemisorption, with the formation of CO as an intermediate. Extensive research by electrochemical methods coupled with species sensitive techniques such as in situ FTIR spectroscopy have shed much light on the latter route. It is generally accepted[15,18] that subsequent to adsorption, three successive dehydrogenation steps lead to the formation of a surface bound intermediate of identity COH or CHO in a process requiring three adjacent Pt sites. Spontaneous and kinetically facile dissociation of this species leads to the formation of strongly adsorbed carbon monoxide (CO_{ads}), which despite being an intermediate for the indirect pathway, may also be considered as the principal poisoning entity, blocking further adsorption of methanol or intermediate fragments at the active sites. Studies suggest that, at room temperature and with dilute electrolyte (0.1 M CH_3OH), methanol adsorption and subsequent dehydrogenation is inhibited when the CO surface abundance reaches 1/3 of a monolayer.[19] Thus for the MOR, the catalyst design challenge involves the minimization of CO surface concentration and/or its rapid removal at the lowest possible overpotential.

The most common approach has been the introduction of atoms of one or more other transition metals onto the surface of platinum. In this respect, Pt−Ru binary catalysts have proven to be very effective for methanol electrooxidation, offering significantly increased currents at low potentials relative to pure Pt.[1,5,20] A recent comprehensive review on Pt−Ru electrocatalysts for fuel cells identified over one thousand relevant articles in the literature.[20] The principal preparatory methods of Pt−Ru binary catalyst systems include electrochemical codeposition, electrodeposition of Ru onto Pt, alloying by thermal decomposition of precursors, and adlayer deposition. The latter approach was pioneered by Watanabe and Motoo,[21] who modified polycrystalline Pt surfaces with adsorbed Ru atoms and coined the term "electrocatalysis by adatoms". These early studies inspired a large body of work on the decoration of Pt electrodes (polycrystalline, single crystal, and nanoparticle-based) by foreign metallic adatoms.[22,23] Studies on the electrooxidation of small organic molecules (SOMs) at Ru (submonolayer (ML)) decorated Pt surfaces have been reviewed.[24,25] The surface modification has been achieved by a variety of approaches.[26−36] A ruthenium coverage dependent enhancement in Faradic current for methanol oxidation is generally reported in the lower overpotential region (<0.65 V vs RHE), when comparing the performance of Ru adatom modified electrodes with the corresponding clean Pt surfaces. The degree of enhancement has been shown to be strongly influenced by the underlying surface structure for the basal planes at potentials relevant to the DMFC; both the order of activity and the Ru induced enhancement factor follow the sequence: Pt (111)/Ru > Pt (110)/Ru > Pt (100)/Ru.[26]

Studies have suggested an improvement in MOR current efficiency at Pt electrodes, with increasing surface step site density.[37,38] Despite this, there has been little work on alcohol electrooxidation at Ru decorated high index Pt electrodes. To the best of our knowledge the only contributions in this area are those due to the Baltruschat group, who have studied CO and methanol oxidation at Ru modified Pt(332), Pt(665), and Pt(755) planes,[39,40] and the Feliu group, whose work has focused on the electrooxidation of ethanol at decorated Pt(775) and Pt(332) stepped electrodes.[35,41]

In this article, we detail the modification of the high index faceted surfaces of THH Pt NCs by various coverages of Ru adatoms, to facilitate a study of methanol and CO electrooxidation on decorated THH Pt NCs with stepped Pt crystal planes. Significantly, this is the first study of a model electrocatalyst constructed by Ru addition to open Pt surfaces lying in the [001] crystallographic zone. Recently, we reported that Bi adatom decoration of THH Pt NCs can induce up to a 70-fold increase in formic acid oxidation current at 0.4 V (RHE).[42] The present study adds a further layer of sophistication, by, for the first time, applying in situ FTIR techniques to probe electrocatalytic reactions occurring at THH Pt NCs deposited on glassy carbon electrodes.

2. EXPERIMENTAL SECTION

2.1. Materials and Apparatus. K_2PtCl_6 (99.99%, Sigma Aldrich), ascorbic acid (99%, Alfa Aesar), sulfuric acid (96%, Merck), perchloric acid (super pure), methanol (A.R. reagent), and $RuCl_3{\cdot}xH_2O$ (pure, latter three from China Medicine Shanghai Chemical Reagent Corp.) were used as received. All solutions were prepared using super pure water (18 MΩ cm) from a Milli-Q system. Carbon monoxide gas (99.99%) was from Xiamen, Xinhang Co.

Glassy carbon (GC) rod (Φ = 6 mm) served as the working electrode substrate. Prior to electro-deposition of the active material, it was polished by successively using alumina powder of sizes 5, 1, and 0.3 μm, and finally cleaned ultrasonically. The electrochemical experiments were conducted at room temperature (~25 °C) in a standard three electrode cell. Platinum foil was employed as the counter electrode, while a saturated calomel electrode (SCE) was used as the reference and all potentials are quoted against this system. Potential control was achieved with a PAR 263A potentiostat/galvanostat operated through home-developed software. All solutions were purged with a stream of pure N_2 gas (99.99%) for 15 min prior to experiments, with a blanket of nitrogen maintained above the electrolyte during measurement to prevent the interference of atmospheric oxygen.

2.2. Preparation of THH Pt Nanocrystals. THH Pt NCs was prepared according to the method reported previously.[11] Briefly, Pt nuclei were first deposited on the GC electrode by applying a potential step from 1.20 V to a reduction potential of −0.24 V, and holding for 20 ms in 2 mM K_2PtCl_6 + 0.5 M H_2SO_4 solution. A square wave potential perturbation of frequency 100 Hz between limits of 0.24 and 0.60 V was then applied for 30 min to affect the growth of polycrystalline Pt nanospheres. Following this, the electrode was transferred to 30 mM ascorbic acid + 0.1 M H_2SO_4 solution, and the nanospheres were subjected to a 10 Hz square wave potential with lower limit of −0.20 V and upper limit of 1.20 V, for a duration of 30 min. Single crystal THH Pt NCs, with a narrow size distribution, were formed at the expense of the nanospheres, as a result of the dynamic interplay of dissolution at the positive extreme and recrystallization at the negative limit. The as-produced THH Pt NC deposit was characterized voltammetrically in 0.1 M H_2SO_4 solution and then imaged by scanning electron microscopy (SEM, Hitachi S-4800).

2.3. Ru Decoration and Methanol Oxidation on THH Pt NCs. The decoration of ruthenium on the THH Pt NC electrode was performed by cyclic voltammetry (CV) in 5×10^{-5} M $RuCl_3$ + 0.1 M $HClO_4$ solution over a potential range of −0.24 to 0.65 V at scan rate of 50 mV s^{-1}, following the method of Del Colle et al.,[35] to deposit Ru on single crystal Pt

dx.doi.org/10.1021/cs200686a | ACS Catal. 2012, 2, 708−715

electrodes. In a typical experiment a low surface coverage of Ru was initially achieved by performing several potential cycles. The surface was then characterized by cyclic voltammetry in 0.1 M H_2SO_4 to evaluate the Ru coverage. Subsequent to this, the electrode was transferred to a cell containing 1.0 M CH_3OH + 0.1 M $HClO_4$ solution. The activity for methanol oxidation was measured, first, via cyclic voltammetry (−0.24 to 0.65 V, 50 mV s^{-1}) and, second, through chronoamperometry, following a potential program outlined in Supporting Information, Figure S1.1. Since the Ru coverage increases with increasing number of potential cycles in the $RuCl_3$ solution, the above steps were repeated a number of times to generate comprehensive data on the variation of methanol electro-oxidation performance with changing Ru adlayer coverage.

The electro-oxidation of CO at the various Ru coverages was also quantified by performing stripping voltammetry measurements in another cell with 0.1 M H_2SO_4 solution. The detailed method for these experiments, including the procedure for saturating the active surface with CO, is outlined in the Supporting Information, Section S2.

The electrocatalytic performance of the Ru decorated THH Pt NCs was compared to those of a commercial carbon supported Pt/Ru (~1:1) alloy catalyst (HiSpec 5000, 20 wt % Pt, 10 wt % Ru, Alfa Aesar) and also Ru modified commercial Pt black (Alfa Aesar). The Ru decoration procedure for the latter was identical to that outlined for the THH material. The details of the preparation of GC electrodes loaded with these commercial catalysts are included in the Supporting Information, Section S3.

2.4. Electrochemical in Situ FTIR Reflection Spectroscopy. In situ IR spectroscopy experiments were carried out with a Nexus 870 FTIR spectrometer (Nicolet) equipped with a liquid-nitrogen-cooled MCT-A detector. The details of the thin layer IR cell have been presented previously.[43] In this configuration, unpolarized IR radiation was sequentially passed through a CaF_2 window and a solution thin layer (~10 μm), prior to reflection by the electrode surface. For each spectrum, 400 interferograms were added to increase the signal-to-noise ratio, while the collection resolution was 8 cm^{-1}. A reference spectrum was acquired at −0.20 V, and the sample spectra were recorded after successive 50 mV potential steps in the direction of increasing potential from 0.05 to 0.35 V. The resulting spectra are reported as relative change in reflectivity, that is,

$$\frac{\Delta R}{R}(E_S) = \frac{R(E_S) - R(E_R)}{R(E_R)}$$

where $R(E_S)$ and $R(E_R)$ are the single-beam spectra collected at the sample potential E_S and reference potential E_R. In this treatment, negative and positive bands indicate respectively, the production and consumption of species at the measurement potential. It is worthwhile pointing out that the FTIR reflection spectroscopy method we used can detect both the adsorbed and the solution species, though it may have a relative low sensitivity for the determination of adsorbed species in comparison with the ATR-SEIRAS.[44]

Time-resolved in situ FTIR spectra were also collected: for these experiments each spectrum is the addition of 20 interferograms with a resolution of 16 cm^{-1}. The reference spectra were acquired at −0.20 V, while the sample spectra were measured at 0.15 and 0.25 V.

3. RESULTS AND DISCUSSION

3.1. THH Pt NCs and Their Modification with Ru. Presented in Figure 1 are CVs characterizing a THH Pt NC

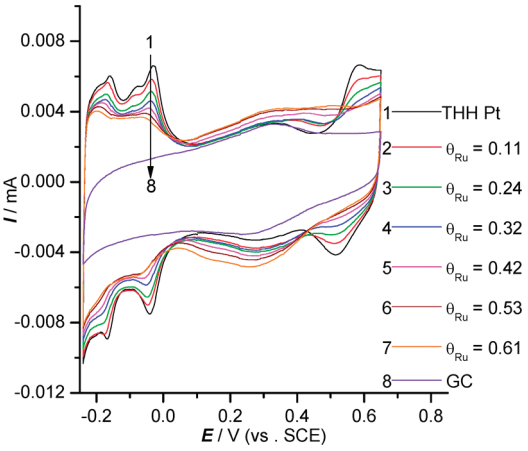

Figure 1. CVs of the THH Pt NC electrodes with various coverages of Ru adatoms, recorded in 0.1 M H_2SO_4 solution at a scan rate of 50 mV s^{-1}.

electrode with various surface coverages of Ru. To avoid Ru atom desorption, the upper potential limit was restricted to 0.65 V. The voltammogram for the unmodified Pt NC material exhibits strong current peaks in the oxygen adsorption/desorption region (>0.46 V), which were not observed in the case of the precursor polycrystalline nanospheres. These enhanced voltammetric features are typical of THH Pt NCs and are indicative of oxygen adsorption at step sites on high index facets.[11]

For each modification, a ruthenium fractional coverage, θ_{Ru}, can be equated with the degree of blockage of hydrogen adsorption sites, and is defined as

$$\theta_{Ru} = 1 - \theta_H = 1 - \frac{Q_H^{Ru}}{Q_H^{unm}}$$

where Q_H^{Ru} is the integrated hydrogen adsorption charge on the Ru modified THH Pt NCs, and Q_H^{unm} is the corresponding charge for bare THH Pt NCs. The integrations were performed between −0.24 and 0.05 V with subtraction of the background charge due to the GC substrate. In addition to the diminishment of the peaks in the hydrogen region, the oxygen adsorption/desorption currents decline rapidly as more Ru is added to the surface. This suggests the displacement of adsorbed oxygen by Ru at Pt step atoms and is consistent with previous observations and predictions,[35,39,40] that the adatoms deposit preferentially at step sites on high index Pt planes. It is thought that an isolated Ru adatom occupying a 4-fold (110) step site will block H adsorption at four Pt atoms at very low Ru coverage (the ratio of blocked hydrogen adsorption sites to Ru adatoms will be 4:1), and an isolated pair of Ru atoms adsorbed on adjacent 4-fold step sites will block an average of three Pt sites each (3:1), and Ru adatoms in a continuous row block an average of two hydrogen adsorption sites (2:1). More detailed discussion of Ru decoration on stepped Pt surface is given in Supporting Information, section S4. Increasing Ru coverage is also accompanied by the broadening of the double layer region, a process well-known for Pt−Ru materials and

dx.doi.org/10.1021/cs200686a | ACS Catal. 2012, 2, 708−715

associated with the onset of OH adsorption by the adatoms.[29,35,40]

3.2. Methanol Electrooxidation on the Ru Modified THH Pt NCs. Voltammograms are presented in Figure 2

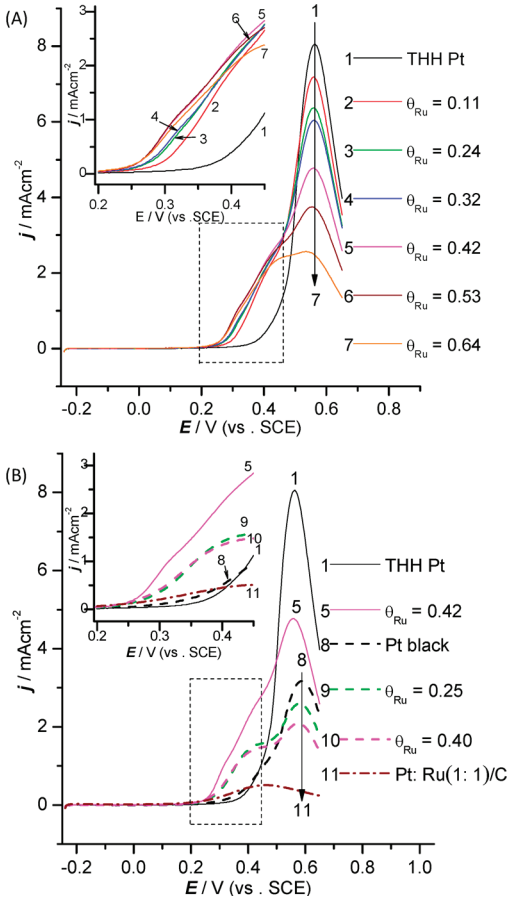

Figure 2. (A) Positive segments of CVs characterizing the methanol electrooxidation performance of Ru decorated THH Pt NCs. (B) Comparison of positive segments of CVs for methanol oxidation on Ru decorated THH Pt NCs(solid line), Ru decorated Pt black (dashed line), and PtRu/C catalyst (dashed-dotted line). The test solution was 1.0 M CH_3OH + 0.1 M $HClO_4$, and the scan rate was 50 mV s^{-1}.

characterizing methanol oxidation at clean and Ru modified THH Pt NCs and Pt black electrodes, and at the commercial PtRu/C electrode. For clarity, only the segments in the positive direction are depicted; the complete profiles are available in the Supporting Information, Figure S6.1. For the THH Pt and Pt black electrodes the currents are normalized to the electroactive surface area (ESA) determined from the hydrogen adsorption charge of the relevant bare electrode. The mass specific electrocatalytic activity is shown in the Supporting Information, Figure S6.2. Examination of the lower potential region, magnified in the inset to Figure 2B, shows, that for the undecorated catalysts the methanol oxidation onset potential follows the sequence PtRu/C < Pt black < THH Pt. The rate of current increase following onset is, however, more rapid for the THH NCs and consequently this electrode exhibits much superior activity for E > 0.45 V than the other two catalysts.

Ru decoration of the THH Pt NCs, and of the Pt black, dramatically reduces the onset potentials for these catalysts, making them comparable to that of the PtRu alloy material. The reduction of onset potentials becomes large as the coverage of Ru increase. But this change becomes unclear for THH Pt NCs electrodes with a high θ_{Ru} (e.g., θ_{Ru} > 0.42). Methanol oxidation commences at 0.23 V for the THH electrode with θ_{Ru} = 0.42, more than 100 mV shifted negatively compared with the same electrode when unmodified. As a result of this lowering in onset potential, the modified Pt black and (especially) THH electrodes offer significantly higher MOR activity than the commercial PtRu/C for potentials above 0.25 V. The modified THH Pt NCs electrode shows higher catalytic current density than the modified Pt black catalyst with similar θ_{Ru} and commercial PtRu/C catalyst. For E = 0.40 V, the catalytic current density for the θ_{Ru} = 0.42 THH Pt NCs electrode is about 66% greater than that of the θ_{Ru} = 0.40 Pt black catalyst, and over four times that of the PtRu/C material. Interestingly for the latter, the peak current is observed at about 0.45 V, which coincides with a shoulder in the current profiles for the modified THH Pt and Pt black electrodes. Notwithstanding the Ru induced catalytic improvement below 0.5 V, the highest peak current density (at ca. 0.55 V) is exhibited by the unmodified THH Pt NCs; as with the onset potential, this quantity diminishes with increasing Ru decoration.

To gain further insight into the effect of the Ru decoration on methanol oxidation, chronoamperometry measurements were conducted on the various electrodes at potentials of 0.20, 0.25, 0.30, and 0.35 V. Figure 3A shows the current density transient (j-t) curves recorded at 0.25 V in 1.0 M CH_3OH + 0.1 M $HClO_4$ solution, from which has been subtracted the background current caused by trace dissolved oxygen reduction in solution (detailed description is shown in Supporting Information, S6). The data acquired at the test potentials is conveniently summarized in Supporting Information, Figure S6.3. The electrocatalytic activities of the Pt catalysts improve progressively with the amount of Ru adatom coverage, in agreement with the cyclic voltammetry data of Figure 2. In the case of the Ru decorated THH Pt NCs, for $\theta_{Ru} \geq$ 0.42, the MOR performance is superior to that of the carbon supported PtRu alloy across the entire studied potential range.

A better appreciation of the potential dependence of the Ru induced oxidation current improvement effect can be obtained by considering the *enhancement factor R*, which is the ratio for a given potential, of the current density recorded at a decorated electrode to that of the clean Pt electrode. From the plot of Figure 3B, it is apparent that, for the Ru decorated THH Pt electrodes and the Pt black catalyst, R increases with increasing Ru coverage at a given potential, especially for $E \leq$ 0.30 V. While R decreases with increasing potential at the same Ru coverage, which indicates that the surface poisoning effect of the catalyst is more obvious at low potential than that at high potential. The Ru decorated THH Pt NCs show higher increase (R) at a low potential than that of Pt black. The largest R was 23, appeared at 0.20 V for THH Pt electrode with θ_{Ru} = 0.64. The R value is 9.7 for the θ_{Ru} = 0.35 THH electrode, and 6.2 for Pt black electrode with similar Ru coverage (θ_{Ru} = 0.36). The larger R value for THH Pt electrode may be because the high-index faceted THH Pt NCs have more steps than Pt black, and are prone to be poisoned at low potential.[13,14] The modified Ru adatoms may preferentially adsorb on the Pt stepped sites, to reduce the poisoning on THH Pt NCs. The ability of Ru adatoms to promote the MOR catalytic activity of Pt nanoparticles with stepped surfaces at low potentials is particularly relevant to fuel cell application, since it is at such

dx.doi.org/10.1021/cs200686a | ACS Catal. 2012, 2, 708–715

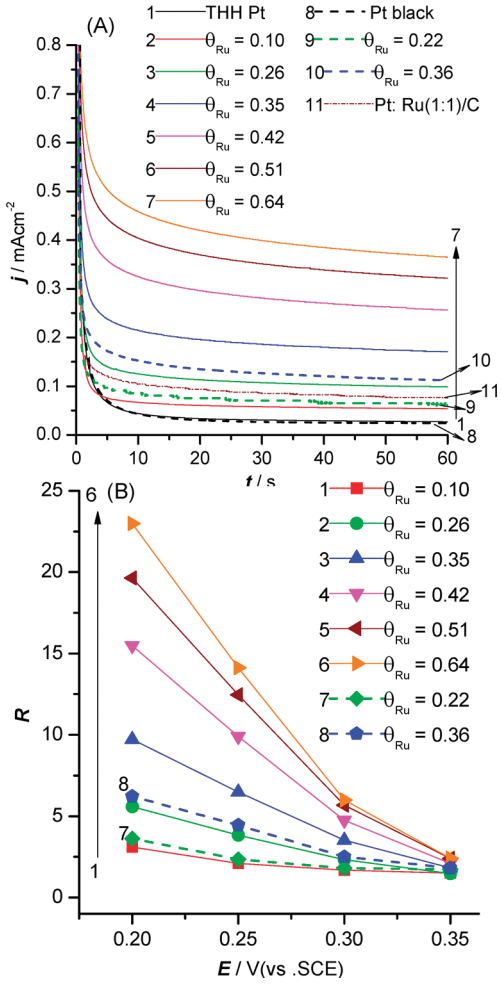

Figure 3. (A) Comparison of chronoamperometric current transients recorded at 0.25 V in 1.0 M CH_3OH + 0.1 M $HClO_4$ solution for the various THH Pt NC (solid line), Pt black (dashed line) and PtRu/C (dashed-dotted line) electrodes. (B) Potential dependence of the enhancement factor *R*. For each Ru decorated Pt electrode, *R* is the ratio of the chronoamperometric current density (from Supporting Information, Figure S6.3) to the current density for the relevant clean electrode.

potentials that maximum output power densities can be achieved.

On the basis of the data of Figure 2 and Figure 3, some intuitive comments can be made regarding the effect of Ru adatom decoration on the MOR at THH Pt NC surfaces. The presence of Ru apparently increases the resistance of the Pt surfaces to poisoning (presumably by CO_{ads}) at potentials below those at which significant OH adsorption occurs on pure Pt. For the modified electrodes, there are two distinct oxidation processes as indicated in Figure 2 by the anodic shoulder stretching from approximately 0.25−0.45 V, and the peak at about 0.55 V, which coincides with the peak potential for the clean Pt NCs. The former feature might be attributed to the oxidation of CO_{ads} at Pt sites adjacent to adsorbed Ru atoms.[34] This interpretation is supported by the fact that the current peak for the Pt/Ru alloy, expected to have a relatively homogeneous surface distribution (solid solution) of the two metals, is also observed in this potential range. The more anodic peak arises from CO_{ads} oxidation at Pt sites that are less influenced by adsorbed Ru, hence the decrease in the associated current with increasing θ_{Ru}. These may be terrace sites, since Ru decoration is expected to be more favored at step edges.

A representative SEM image is presented in Figure 4 of the THH Pt NCs with θ_{Ru} = 0.53 after methanol oxidation

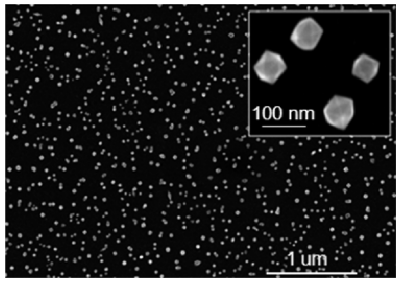

Figure 4. SEM image of THH Pt NCs (θ_{Ru} = 0.53) captured subsequent to methanol electrooxidation studies. The inset is a higher magnification image of the same sample and clearly shows the characteristic THH shape.

experiments. The inset, at higher magnification, clearly exhibits that the crystals are of the THH geometric shape, showing that crystal shape integrity has been preserved through both the Ru deposition process and the electrocatalytic testing. SEM image analysis of a statistically meaningful number of particles (350) reveals a mean diameter of about 55 nm, with 90% of crystals being of THH shape (Supporting Information Figure S5.1,).

3.3. CO Electrooxidation on the Ru Modified THH Pt NCs. The behavior of the modified electrode surfaces regarding the electrooxidation of deliberately adsorbed CO may help to further elucidate the nature of the promotional effect caused by the Ru adatoms. Figure 5 shows the CO stripping voltammo-

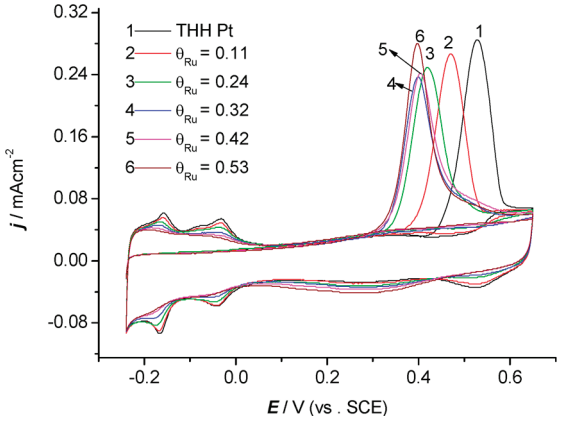

Figure 5. CO oxidative stripping CVs for the bare and Ru decorated THH Pt NC electrodes. The electrolyte solution was 0.1 M H_2SO_4, and the scan rate was 50 mV s^{-1}.

grams for THH Pt NC electrodes with various values of θ_{Ru}. For the clean electrode, the onset potential for CO oxidation is 0.41 V, with the peak observed at about 0.53 V. It is evident that with increasing θ_{Ru}, both the oxidation onset and peak potentials are shifted to more negative values. The bulk of this shift is observed for lower coverages ($\theta_{Ru} \leq 0.24$), mirroring the situation for the decreasing onset potential of methanol oxidation in Figure 2A. For θ_{Ru} = 0.53, the CO oxidation peak potential is decreased by some 130 mV compared to the bare electrode.

dx.doi.org/10.1021/cs200686a | ACS Catal. 2012, 2, 708−715

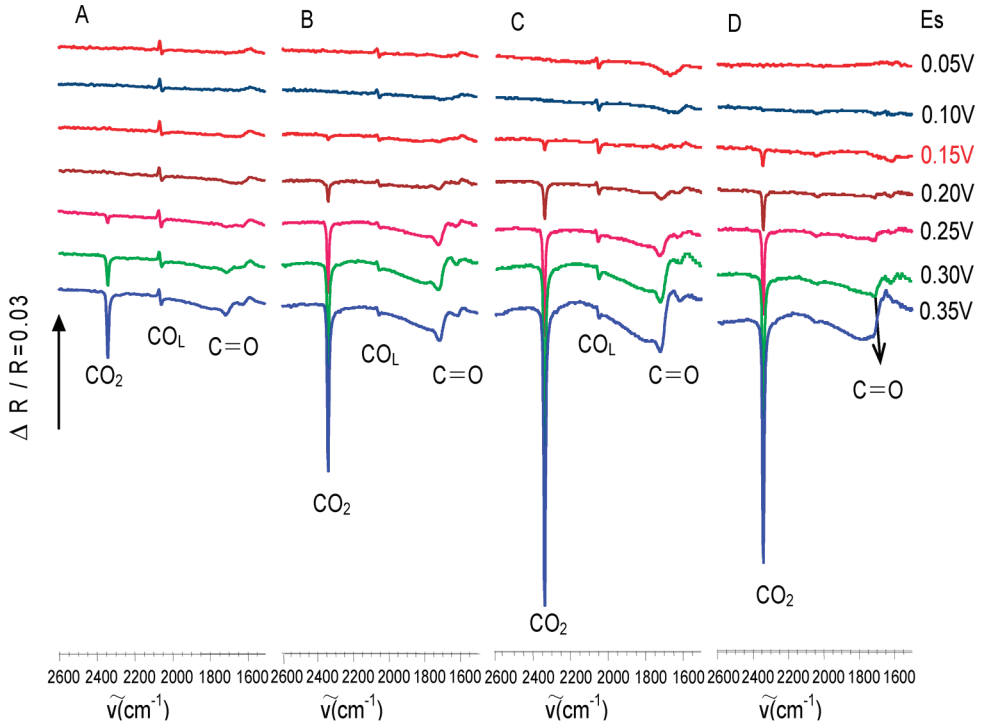

Figure 6. In situ FTIR spectra for methanol electrooxidation on (A) the clean THH Pt NCs electrode, (B) THH Pt NCs electrode (θ_{Ru} = 0.30), (C) THH Pt NCs electrode (θ_{Ru} = 0.49), and (D) commercial PtRu/C catalyst, in 1.0 M CH_3OH + 0.1 M $HClO_4$ solution. The reference spectra were acquired at −0.20 V.

The oxidation of CO at Ru decorated Pt single crystal electrodes and nanoparticles has received considerable attention.[27,29,30,39,45−47] CO stripping voltammograms recorded in H_2SO_4 solution for Ru modified Pt(111) surfaces typically exhibit two oxidation peaks: the lower arises from CO adsorbed at the edges of Ru islands, while the upper results from CO adsorbed at Pt terrace sites away from the Ru clusters.[46,47] This interpretation is supported by the fact that the relative charges associated with the peaks vary with Ru coverage, the upper peak becoming suppressed as the coverage is increased. Although there is clearly no second peak in the stripping CVs of Figure 5, the oxidation peaks are asymmetrical with a tail-like feature evident on the positive edge, at potentials between about 0.47 and 0.55 V for $\theta_{Ru} \geq 0.24$. This situation is comparable with results obtained by Samjeske et al.[39] for CO oxidation at Ru decorated Pt(665) (= [12(111) × (111)]) and (755) (= [6(111) × (100)]) single crystal electrodes. While the upper oxidation peak was clearly in evidence for the Pt(665)/Ru surface, it was greatly suppressed for the Pt(755)/Ru surface with its narrower (111) terraces. Coupling this observation with our data in Figure 5, it seems that a definite higher CO stripping peak is not observed for Ru decoration of stepped Pt surfaces with narrow terraces, since CO_{ads} can never be too distant from the Ru adatoms at the step edges.

Enhancements in Pt electrode performance through the incorporation of foreign metal atoms are usually attributed to one or more of three effects. The third body effect envisages the physical blocking of some active centers, preventing the formation of poisons which require an ensemble of adsorption sites and thereby routing the reaction through a direct (nonpoisoning) pathway. Conversely, the electronic effect hypothesizes that the electronic properties of the catalytic substrate are altered, affecting the enthalpy of adsorption of intermediates or poisoning entities. For PtRu electrocatalysts, activity improvements relative to pure Pt are usually explained by the so-called bifunctional mechanism.[21] According to this theory, Ru (being less noble than Pt) activates H_2O and adsorbs OH species at lower potentials than are possible for Pt. The adsorbed CO at the Pt sites then reacts with the OH adsorbate at the Ru centers through a Langmuir−Hinshelwood mechanism, producing CO_2 and concomitantly liberating the metal atoms for further adsorption.

The decrease in onset and peak potentials for CO oxidation with increasing θ_{Ru}, evident in Figure 5, is reminiscent of results reported by other authors for Ru decorated Pt.[30,46,47] According to the analysis of Davis et al.,[46] such behavior is strongly indicative of activity promotion via the bifunctional mechanism. In the present case, the lowering of the overpotential for CO_{ads} oxidation is clear evidence that Ru adatoms are not merely site blockers, but active participants in the oxidative removal of CO.

3.4. In Situ FTIR Spectroscopy Studies. In situ FTIR spectroscopy was utilized to further understand the promotional effect of Ru adatoms on the MOR activity, since this technique is sensitive to the chemical identity of significant intermediates and products at the catalyst surface as the reaction proceeds. FTIR spectra recorded in 1.0 M CH_3OH + 0.1 M $HClO_4$ are presented respectively in Figures 6A−D, for the clean THH NC electrode, THH NC electrodes with θ_{Ru} values of 0.30 and 0.49, and for the commercial carbon supported 1:1 Pt/Ru alloy catalyst. The negative band near 2343 cm^{-1} is due to CO_2 formation.[28] The band at about 1710 cm^{-1} is associated with formic acid, or more specifically, methyl formate, $HCOOCH_3$ in solution, which forms rapidly from HCOOH in the presence of methanol.[48] Linearly bonded CO_{ads} gives rise to the band observed at about 2050 cm^{-1}. Direct visual comparison can be made between the band intensities in Figures 6A−C. It should, however, be kept in

dx.doi.org/10.1021/cs200686a | ACS Catal. 2012, 2, 708−715

mind that the active surface area of the PtRu/C electrode is different (slightly larger) than that of the THH Pt NCs electrode, so the intensities in D are not directly comparable with A–C.

The bipolar nature of the CO_{ads} feature in Figures 6A–C is indicative of the fact that this adsorbate is present at both the reference and the sample potentials, with the characteristic frequency showing a potential dependent shift (Stark effect). This implies that dissociative adsorption of methanol to form CO_{ads} occurs even at −0.20 V for the THH Pt NC electrodes. By contrast there is evidently no adsorbed CO present on the surface of the PtRu/C electrode at the reference potential: a slight negative depression in the spectrum recorded at 0.10 V (Figure 6D) suggests the onset of some CO adsorption from this potential. However, the intensity of this band remains minimal as the potential is increased.

The effect of Ru decoration on the THH Pt NCs is most obvious from the appearance of a CO_2 signal (2343 cm^{-1}) at 0.15 V for the modified electrodes (Figures 6 B and C), some 100 mV lower than the onset of the same band for the clean electrode. This is in strong accord with the voltammetric results of Figure 2A, which showed a decrease in oxidation current onset potential of over 100 mV following Ru modification of the THH surface. For the decorated electrodes, the CO_2 band is followed 50 mV later by the C═O stretching mode signal characteristic of formic acid production due to methanol oxidation via the direct (non-poisoning) pathway. As with the modified THH surfaces, CO_2 production is first observed at 0.15 V for the commercial PtRu material: again this is consistent with the voltammetric data of Figure 2B as discussed in section 3.2.

Some qualitative differences in the spectra for the Ru decorated THH Pt NCs and the PtRu/C catalyst merit comment. While the CO_{ads} band intensity is virtually negligible for the alloy material, in the case of the decorated electrodes there is a small but distinct signal for this species at all potentials above the onset of CO_2 production. This signal is likely to arise mainly from CO adsorbed at terrace sites not adjacent to Ru adatoms, a concept previously discussed in relation to the MOR voltammetry and CO stripping data. Furthermore it is noteworthy that for $0.2 \leq E \leq 0.3$ V, the intensity of the formic acid bands relative to the CO_2 bands is greater in Figures 6 B and C than in D. This suggests that over this potential range, the direct methanol oxidation pathway via formic acid is more significant for the decorated stepped surfaces of the THH electrodes than for the PtRu alloy. Ru modification of the THH Pt NCs not only enhances the yield of CO_2 through CO_{ads} oxidation, but some of the Pt sites vacated in the process become available for methanol oxidation through the formic acid route.

To put these FTIR results on a quantitative footing, Figure 7 presents plots of the integrated intensity of the ~2343 cm^{-1} CO_2 band against potential for each of the four electrodes. The data has been normalized to the electroactive surface area. It is evident that the decorated THH electrodes are more efficient at producing CO_2 than the PtRu alloy at potentials including, and above 0.15 V for θ_{Ru} = 0.49, or 0.20 V for θ_{Ru} = 0.30.

The spectra of Figure 6 offer a time averaged perspective on the formation of intermediates and products at the surface of the electrodes. Further useful information can be obtained by monitoring the temporal evolution of the FTIR response at a given potential. To this end, time-resolved spectra recorded at 7.63 s intervals at a potential of 0.25 and 0.15 V are presented

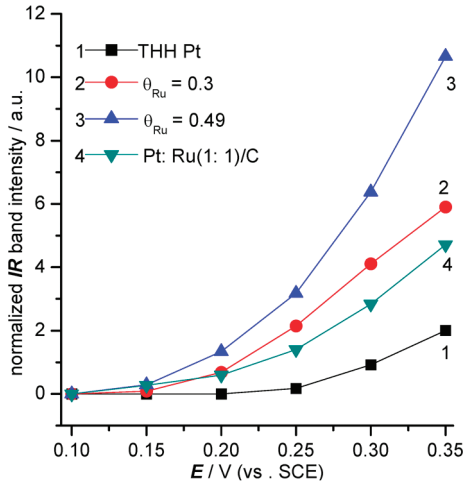

Figure 7. Variation, with applied potential, of the integrated intensity (I) of the ~2343 cm^{-1} CO_2 band extracted from the spectra of Figure 6. The data was normalized to the electrochemical active surface area of the relevant electrode. An un-normalized version of this plot is presented in the Supporting Information, Figure S7.1.

in the Supporting Information, Figures S7.2 and Figure S7.3, respectively. This data shows that CO_2 production is more facile at the modified THH surfaces than at the alloy surface. The amount of CO_2 accumulated after 148 s in the electrolyte thin layer per unit catalyst surface area is approximately three times greater for the Ru decorated (θ_{Ru} = 0.49) Pt THH NCs material than for the commercial PtRu/C catalyst. The time-resolved spectra also highlight the enhanced selectivity for formic acid production of the decorated high index faceted surfaces when compared to the PtRu alloy.

4. CONCLUSIONS

THH Pt NCs were decorated by Ru adatoms through electrochemical deposition. The effect of the adatoms on the surface electrochemistry was evaluated by cyclic voltammetry. The degree of reduction in the hydrogen adsorption peaks is related to the extent of Ru coverage. Ru decoration lowers the onset potential of methanol oxidation at the THH Pt NCs ($\theta_{Ru} \geqslant 0.42$) by over 100 mV, to a value comparable with that displayed by a commercial carbon supported PtRu alloy nanoparticle catalyst. Following onset, the catalytic current density is much higher for the Ru decorated THH Pt NCs, than for either a Pt black catalyst with similar Ru coverage or the PtRu/C material. A progressive negative shift, with increasing Ru coverage, in the potential for CO oxidation in stripping voltammetry experiments suggests that the Ru adatom induced catalytic enhancement is mainly attributable to the bifunctional mechanism.

FTIR studies reveal that Ru decorated THH Pt NCs (θ_{Ru} = 0.49) are a more efficient catalyst for the production of CO_2 than the PtRu/C material at all potentials above 0.15 V. Methanol oxidation via the non-poisoning path through formic acid is also more favored for the decorated THH NCs, relative to the commercial PtRu/C nanoparticles. The ability of Ru modified, high index faceted, Pt nanocrystals to outperform the industry standard MOR electrocatalyst at low overpotentials is particularly significant in the development of next generation anodic catalysts for direct methanol fuel cells.

dx.doi.org/10.1021/cs200686a | ACS Catal. 2012, 2, 708–715

■ ASSOCIATED CONTENT

Supporting Information

Extra detail on the experimental procedures, additional cyclic voltammetry and chronoamperometry data, additional in situ FTIR data, and time resolved in situ FTIR spectra. This material is available free of charge via the Internet at http://pubs.acs.org.

■ AUTHOR INFORMATION

Corresponding Author

*E-mail: tnsd@xmu.edu.cn (N.T.), sgsun@xmu.edu.cn (S.-G.S.), w.lin@qub.ac.uk (W.-F.L.).

Funding

This study was supported by NSFC (21021002, 20933004, 21073152, and 20873113), the Fundamental Research Funds for the Central Universities (2010121021) and Program for New Century Excellent Talents in University. M.P.B., C.H., and W.-F.L. gratefully acknowledge financial support from Queen's University Belfast (The ISW DEL Clean Energies) and the EPSRC (EP/I013229/1).

Notes

The authors declare no competing financial interest.

■ REFERENCES

(1) Wasmus, S.; Küver, A. *J. Electroanal. Chem.* **1999**, *461*, 14−31.
(2) Aricò, A. S.; Srinivasan, S.; Antonucci, V. *Fuel Cells* **2001**, *1*, 133−161.
(3) Lamy, C.; Lima, A.; LeRhun, V.; Delime, F.; Coutanceau, C.; Leger, J.-M. *J. Power Sources* **2002**, *105*, 283−296.
(4) Kamarudin, S. K.; Daud, W. R. W.; Ho, S. L.; Hasran, U. A. *J. Power Sources* **2007**, *163*, 743−754.
(5) Zhao, X.; Yin, M.; Ma, L.; Liang, L.; Liu, C.; Liao, J.; Lu, T.; Xing, W. *Energy Environ. Sci.* **2011**, *4*, 2736−2753.
(6) Dillon, R.; Srinivasan, S.; Aricò, A. S.; Antonucci, V. *J. Power Sources* **2004**, *127*, 112−126.
(7) Koenigsmann, C.; Wong, S. S. *Energy Environ. Sci.* **2011**, *4*, 1161−1176.
(8) Kamarudin, S. K.; Achmad, F.; Daud, W. R. W. *Int. J. Hydrogen Energy* **2009**, *34*, 6902−6916.
(9) Zhou, Z.-Y.; Tian, N.; Huang, Z.-Z.; Chen, D.-J.; Sun, S.-G. *Faraday Discuss.* **2008**, *140*, 81−92.
(10) Zhou, Z.-Y.; Tian, N.; Li, J.-T.; Broadwell, I.; Sun, S.-G. *Chem. Soc. Rev.* **2011**, *40*, 4167−4185.
(11) Tian, N.; Zhou, Z.-Y.; Sun, S.-G.; Ding, Y.; Wang, Z. L. *Science* **2007**, *316*, 732−735.
(12) Sun, S.-G.; Chen, A.-C.; Huang, T.-S.; Li, J.-B.; Tian, Z.-W. *J. Electroanal. Chem.* **1992**, *340*, 213−226.
(13) Tian, N.; Zhou, Z.-Y.; Sun, S.-G. *J. Phys. Chem. C* **2008**, *112*, 19801−19817.
(14) Zhu, T.; Tian, N.; Kong, D.; Sun, S. *Sci. China, Ser. B: Chem.* **2009**, *52*, 1660−1665.
(15) Iwasita, T. *Electrochim. Acta* **2002**, *47*, 3663−3674.
(16) Kauranen, P. S.; Skou, E.; Munk, J. *J. Electroanal. Chem.* **1996**, *404*, 1−13.
(17) Breiter, M. W. *Electrochim. Acta* **1967**, *12*, 1213−1218.
(18) Lamy, C.; Léger, J.-M.; Srinivasan, S. In *Modern Aspects of Electrochemistry*; Bockris, J. O. M., Conway, B. E., White, R. E., Eds.; Kluwer: New York, 2002; Vol. *34*, pp 53−118.
(19) Jusys, Z.; Behm, R. J. *J. Phys. Chem. B* **2001**, *105*, 10874−10883.
(20) Petrii, O. *J. Solid State Electrochem.* **2008**, *12*, 609−642.
(21) Watanabe, M.; Motoo, S. *J. Electroanal. Chem.* **1975**, *60*, 275−283.
(22) Markovic, N. M.; Ross, P. N. *Surf. Sci. Reports* **2002**, *45*, 117−229.
(23) Spendelow, J. S.; Wieckowski, A. *Phys. Chem. Chem. Phys.* **2004**, *6*, 5094−5118.
(24) Maillard, F.; Lu, G. Q.; Wieckowski, A.; Stimming, U. *J. Phys. Chem. B* **2005**, *109*, 16230−16243.
(25) Spendelow, J. S.; Babu, P. K.; Wieckowski, A. *Curr. Opin. Solid State Mater. Sci.* **2005**, *9*, 37−48.
(26) Chrzanowski, W.; Wieckowski, A. *Langmuir* **1998**, *14*, 1967−1970.
(27) Lin, W. F.; Zei, M. S.; Eiswirth, M.; Ertl, G.; Iwasita, T.; Vielstich, W. *J. Phys. Chem. B* **1999**, *103*, 6968−6977.
(28) Iwasita, T.; Hoster, H.; John-Anacker, A.; Lin, W. F.; Vielstich, W. *Langmuir* **2000**, *16*, 522−529.
(29) Waszczuk, P.; Solla-Gull, J.; Kim, H. S.; Tong, Y. Y.; Montiel, V.; Aldaz, A.; Wieckowski, A. *J. Catal.* **2001**, *203*, 1−6.
(30) Tong, Y.; Kim, H. S.; Babu, P. K.; Waszczuk, P.; Wieckowski, A.; Oldfield, E. *J. Am. Chem. Soc.* **2002**, *124*, 468−473.
(31) Christensen, P. A.; Jin, J.-M.; Lin, W.-F.; Hamnett, A. *J. Phys. Chem. B* **2004**, *108*, 3391−3394.
(32) El-Shafei, A. A.; Hoyer, R.; Kibler, L. A.; Kolb, D. M. *J. Electrochem. Soc.* **2004**, *151*, F141−F145.
(33) Yee, N.; Chottiner, G. S.; Scherson, D. A. *J. Phys. Chem. B* **2004**, *108*, 5847−5850.
(34) Wei, Z. D.; Li, L. L.; Luo, Y. H.; Yan, C.; Sun, C. X.; Yin, G. Z.; Shen, P. K. *J. Phys. Chem. B* **2006**, *110*, 26055−26061.
(35) Del Colle, V.; Berna, A.; Tremiliosi-Filho, G.; Herrero, E.; Feliu, J. M. *Phys. Chem. Chem. Phys.* **2008**, *10*, 3766−3773.
(36) Arruda, T. M.; Shyam, B.; Lawton, J. S.; Ramaswamy, N.; Budil, D. E.; Ramaker, D. E.; Mukerjee, S. *J. Phys. Chem. C* **2010**, *114*, 1028−1040.
(37) Shin, J.; Korzeniewski, C. *J. Phys. Chem.* **1995**, *99*, 3419−3422.
(38) Housmans, T. H. M.; Koper, M. T. M. *J. Phys. Chem. B* **2003**, *107*, 8557−8567.
(39) Samjeske, G.; Xiao, X.-Y.; Baltruschat, H. *Langmuir* **2002**, *18*, 4659−4666.
(40) Wang, H.; Baltruschat, H. *J. Phys. Chem. C* **2007**, *111*, 7038−7048.
(41) Souza-Garcia, J.; Herrero, E.; Feliu, J. M. *ChemPhysChem* **2010**, *11*, 1391−1394.
(42) Chen, Q.-S.; Zhou, Z.-Y.; Vidal-Iglesias, F. J.; Solla-Gull, J.; Feliu, J. M.; Sun, S.-G. *J. Am. Chem. Soc.* **2011**, *133*, 12930−12933.
(43) Li, J.-T.; Chen, Q.-S.; Sun, S.-G. *Electrochim. Acta* **1997**, *52*, 5725−5732.
(44) Zhang, H.-X.; Wang, S.-H.; Jiang, K.; André, T.; Cai, W.-B. *J Power Sources* **2012**, *199*, 165−169.
(45) Davies, J. C.; Hayden, B. E.; Pegg, D. J. *Electrochim. Acta* **1998**, *44*, 1181−1190.
(46) Davies, J. C.; Hayden, B. E.; Pegg, D. J.; Rendall, M. E. *Surf. Sci.* **2002**, *496*, 110−120.
(47) Lu, G. Q.; Waszczuk, P.; Wieckowski, A. *J. Electroanal. Chem.* **2002**, *532*, 49−55.
(48) Xia, X. H.; Iwasita, T.; Ge, F.; Vielstich, W. *Electrochim. Acta* **1996**, *41*, 711−718.